Analysis of separated 2D flows

ARPAD A. FAY
retired from Flow and Heat Machinery Department,
University of Miskolc, Hungary.
Tó u. 16, Vértessomló, 2823
HUNGARY

Abstract: Essentially 2-dimensional, subsonic, small viscosity (air, water), turbulent, separated flows are discussed. Several well-known flow configurations are analyzed with the aim of understanding the flow mechanisms. For flows around circular cylinders the classical explanation of the flow separation is completed with the Coanda effect. For vortex rows with unidirectional rotations flow separations are explained by Knapp's cycle, for non-cavitating flows as well. For Karman vortex rows the vortex formation is attributed to alternate jet formations. Some of the main conclusions are derived from cavitation tunnel experiments. At the end listing the main physical factors is attempted.

Key-Words: Flow separation, 2D flows, Flows around cylinders, Vortex formation, Cavitating and Non-cavitating vortex rows

1 Introduction

Many efforts are made to compute flows with flow separations [1]. The abundant information even on the tiny details of the flows, however, does not really reveal the fluid mechanical background of these flows. To understand the basic mechanisms one is inclined to return to rational mechanics, the approach which started with Newton and Euler. This paper has been written in an attempt to provide a classical analysis for essentially 2-dimensional, turbulent, small viscosity, separated flows, like those past circular cylinders in air or water tunnels. At first sight cavitating flows seem to be more complicated than flows in air tunnels. Nevertheless, the contribution of the cavitation tunnel experiments to the understanding of 2D flow separations is enormous. This is utilized below.

2 Pelton jet

A jet from a Pelton model turbine nozzle is shown in Fig. 1. A computation assuming incompressible frictionless flow resulted in decreasing radius r with increasing coordinate x. This contradicted to the experiment, where, after the vena contracta, r increased with x as seen in the photo. The discrepancy is caused by the turbulence. The computed jet is circular. The boundary of the real jet is irregular due to turbulence. If a small fluid mass m at jet boundary gets a small velocity component v' perpendicular to the axis, then this mass will continue its motion with its new velocity since in the constant pressure region there is no force to change it. Thus the path of such a particle is a straight line, the photo truly shows this. Further downstream this mass may even depart from the jet as a droplet.

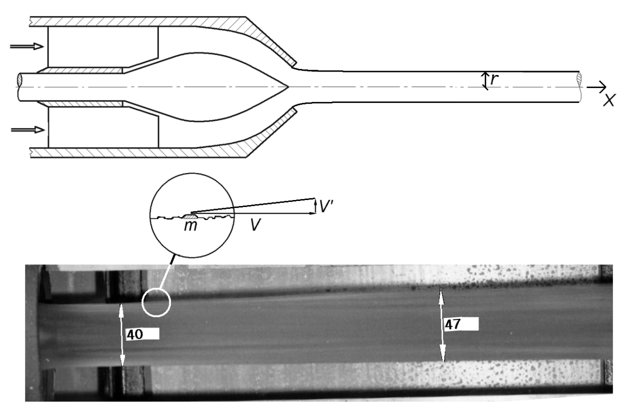

Fig. 1. Pelton jet, photo C. Zombor, permission by him

This case offers an extra opportunity to obtain measures for the turbulence from macroscopic parameters. The angle of the particle path can be measured. Since the jet velocity is known, the turbulent velocity v' can be calculated. Catching the droplets beside the jet may provide information on the size of the region what took this velocity.

3 Flow past circular cylinders

Circular cylinders placed perpendicularly into the main flow offer a splendid example for flow separations. The well-known diagrams are repeated here in Fig. 2.

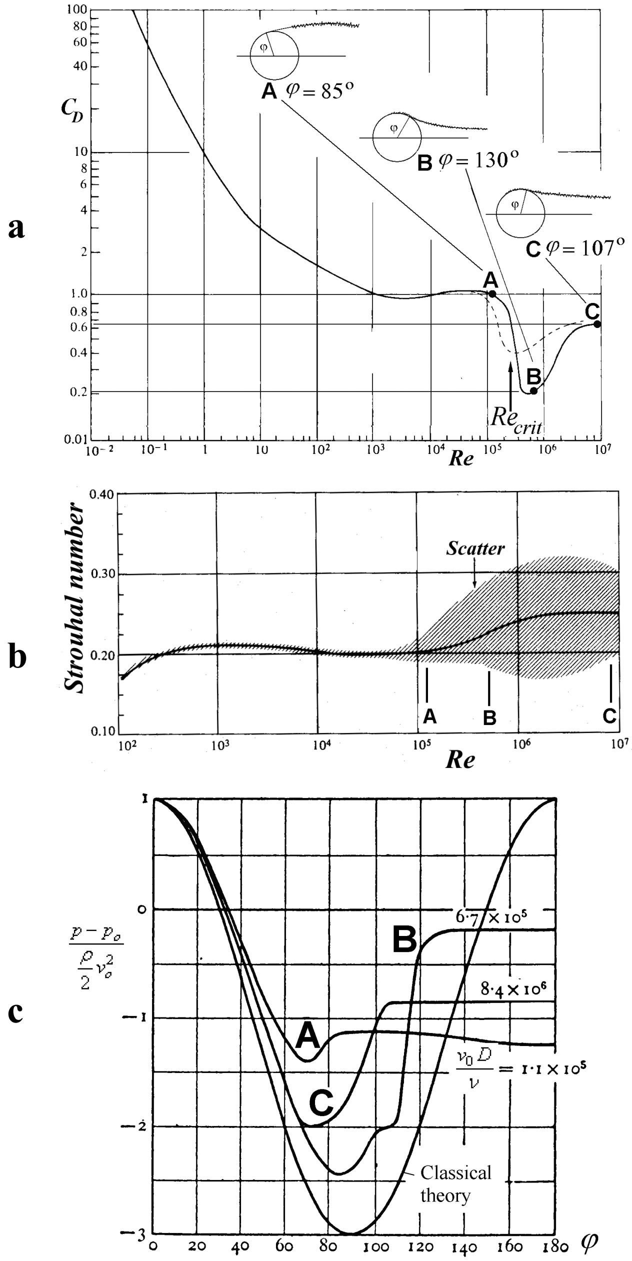

Fig. 2. Flows past cylinders, a, drag coefficient, b, Strouhal number, c, pressure coefficient, after [2] and [3]. φ is the angle from the front stagnation point.

The drastic change in C_D is seen in Fig. 2a at the critical Reynolds number. Three points **A**, **B**, and **C** are noted on the curve where the flow conditions are analyzed. The boundary layers separate in each case. The pressure in the wake regions is nearly constant, as seen in Fig 2c. The separation angles given in Fig. 2a were determined from these pressure distributions at points where the wake pressure is already reached.

These separation angles are not very accurate. At point **A** rather a separation region may be suspected in the range $\varphi = 60$ to 85 degree (Fig. 2c). There is some evidence that the separation point oscillates in this range with the pace of the vortex shedding.

The *Strouhal* number plotted here (Fig. 2b) was calculated from the time periods between shedding vortices. Below $Re = 10^5$ a single curve is obtained. Above this value the shedding becomes irregular. For this an explanation is attempted at the end of the paper.

The classical explanation suggested by Prandtl for the fall of C_D at the Re_{crit} is the following [2]. In the range $Re = 10^3$ to 10^5 the boundary layer separating from the cylinder is laminar. The transition to turbulent boundary layer occurs downstream the separation point. With increasing *Re*, the transition point gradually approaches the separation point, and when it arrives near to the cylinder, the boundary layer adjoins (or reattaches) to the surface of the cylinder. The larger the separation angle the wake becomes narrower (Fig. 2a), and C_D is smaller. However, it is still an open question why the boundary layer adjoins to the surface. For this an explanation is attempted at the end of the paper.

The dotted line in Fig. 2a was obtained with rough cylinder. Roughness brings the transition point nearer to the surface, this is why Re_{crit} became smaller.

4 Inertia separation

For case **A** one is tempted to return to 'inertia separation' introduced by Strscheletzky [4].

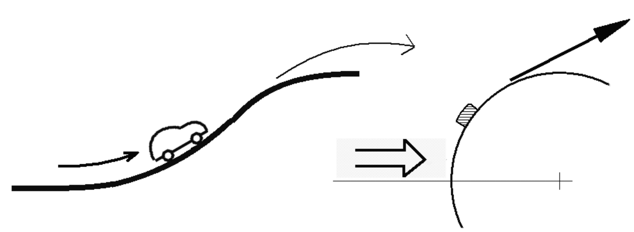

Fig. 3. Analogy for flow separation in Case **A**

The inertia of the fluid masses may be responsible for the flow separation. An analogy is shown in Fig. 3, backing the idea. Strscheletzky derived 'inertia separation' from the Hamiltonian principle of mechanics. The technique [5] is based on calculating the variations of a certain integral over the flow domain. If it is not extremal, then flow separation is predicted. This theory includes, however, a logical 'circulus viciosus'. The Hamiltonian principle is a consequence of the Newtonian laws; therefore it cannot be used to make distinction among flows obeying to the Newtonian laws. Though the theory fails, the idea is part of the truth. Consider a fluid particle (Fig. 3), traveling at the surface of the cylinder but outside the boundary layer. It is pressed to the cylinder by the neighboring particles. However, reaching near to zenith, the pressure becomes less and less, and at a certain point the inertia of the particle may overcome the effect of the pressure, and the particle may leave the surface like the small car in Fig. 3. Thus, inertia plays an important role in flow separations when the boundary layer is laminar. However, the inertia *alone* does not explain separation, since the turbulent boundary layer, under identical inertia conditions outside the boundary layer, does not separate at $\varphi = 85$ degree.

5 Coanda effect

In the boundary configuration of Fig. 4 a jet discharges from a slot into a constant pressure space. The jet is attracted by the wall: this is the Coanda effect.

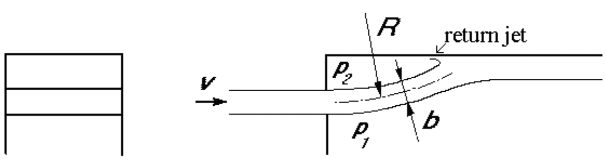

Fig. 4. 2D Coanda effect: the wall attracts the jet.

Considering air flow, the Coanda effect is explained as follows. The turbulent jet diverges (as the Pelton jet). It reaches the wall somewhere, perhaps far away. A closed space is resulted between the jet and the wall. The turbulent jet takes air out of this space, and so its pressure p_2 decreases. It is the pressure differential $p_1 - p_2$ that pulls the jet towards the wall.

The Euler equation may be written for the jet:

$$\frac{v^2}{R} = -\frac{1}{\rho}\frac{\partial p}{\partial n} \cong \frac{p_1 - p_2}{\rho b} \qquad (1)$$

of which it follows that R is nearly constant, the jet is nearly circular. The decreasing p_2 stops at a certain value. Denote by $Q_{turbulence}$ the air volume per unit time carried away by the turbulent jet from the closed space, and by $Q_{return\ jet}$ the air volume per unit time of the return jet (Fig. 4) caused by the main jet attacking the wall at an inclination (what can be calculated easily). The steady flow is determined by the equilibrium:

$$Q_{turbulence} = Q_{return\ jet} \quad . \qquad (2)$$

This shows that turbulent flow computations may be successful for the steady 2D Coanda flow *only if* $Q_{turbulence}$ is reliably determined.

For water jets discharging into water the Coanda effect is still valid, since water is also compressible.

6 Diffuser

Looking at Fig. 5 the Coanda effect is clearly important in diffuser flows. Assuming steady flow, the curvature of the streamlines indicates the presence of a pressure gradient. It seems however, that the experimental evidence of the depression zone on the wall has not been fully explored yet.

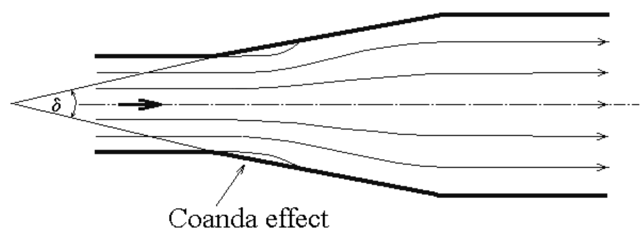

Fig. 5. Flow in a 2D diffuser

7 Borda-Carnot loss

The same is valid for a sudden enlargement of the flow channel as shown in Fig. 6. In this case the flow loss can easily be determined by the Borda-Carnot loss formula what serves well in practice. However, in calculating the boundary layer losses, in most cases these are at a fraction of the Borda-Carnot loss term, and therefore unsteady flow and continuous formation of vortices may be expected, what is again not explored in sufficient details.

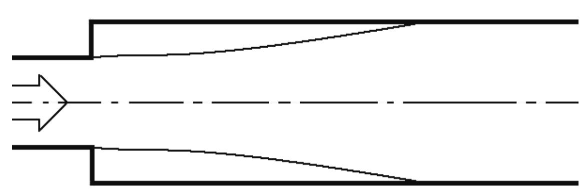

Fig. 6. Sudden enlargement of the flow channel

8 Convergent-divergent channel

The formation of cavitating vortices can be seen in convergent-divergent channels (Fig. 7), which is a simple means to study the mechanism of cavitation on pump or hydroturbine blades.

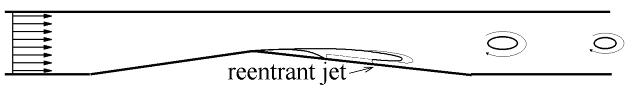

Fig. 7. Cavitating flow in convergent-divergent channel

Knapp determined the life-cycle of such cavities [6], and Furness developed it further [7]. It begins with the formation of a small cavity at the edge. The cavity increases, and a reentrant jet appears at the rear end of the cavity (Fig. 7). The reentrant jet refills the cavity, and when it strikes the liquid-gas interface, a cavity is separated from the main cavity. Later the separated cavity is swept away. At the time of the impact the original cavity disappears, and the cycle begins with the formation. This cavitation cycle at the edge generates a series of vortices, which rotate in the same direction and have cavities in their cores.

Under large pressure in the channel no cavity is formed but vortices still appear at the edge. The non-cavitating vortex formation is very similar to the above one. In this case water occupies the place of the cavity, and this retards the reentrant jet. Therefore the Strouhal number of the non-cavitating vortex shedding is smaller than in the cavitating case.

Thus, in both cavitating and non-cavitating flows, if unidirectional vortex rows are found somewhere, the mechanism of the vortex formation is Knapp's cycle.

9 Karman vortex rows

In the wakes of circular cylinders or other blunt bodies vortices appear rotating alternately. Von Karman developed a stability criterion for such vortex rows but did not dealt with the formation of the vortices. The near-body flow mechanism attracted the attention of many researchers but the subject is not settled yet.

One frame of a high-speed film [8] is shown in Fig. 8. An equilateral wedge model had been placed into the cavitation tunnel which operated at Re = 6.10^5 (above critical) with cavitation number:

$$K = \frac{p_{ref} - p_{vapor}}{\frac{\rho}{2} v_{ref}^2} \cong 1 \tag{3}$$

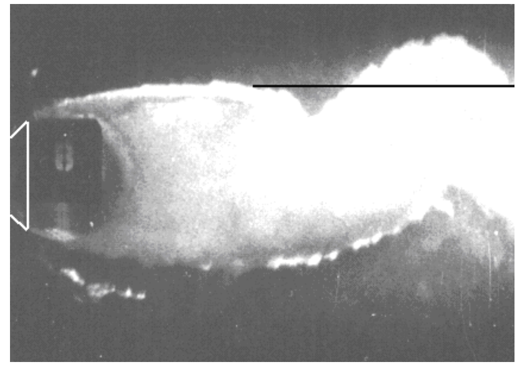

Fig. 8. Cavity downstream a wedge, [8], by permission of Sebestyén

The foam-like substance in the cavity prevents seeing clearly what is happening in the cavity interior. Two intrusions are striking on the cavity boundary, which seem to be the roots of two jets. The presence of the second jet can be deduced from the fact, that the jet pushed the other side of the cavity upwards. The horizontal line drawn in the picture demonstrates the magnitude of the surface displacement. There are signs that the first jet nearer to the wedge also reached the other side of the cavity. A disturbance is seen on the surface, opposite to the root, and subsequent frames of the film show that the surface begun to be displaced in this region. Thus the presence of jets has been deduced.

The development of the deduced downward jet is sketched in Fig. 9. Fig. 8 is similar to Fig 9b. Since Fig. 9e is the mirror of Fig. 9a, the upward jet starts. Thus, the mechanism is explained by alternate jet formations.

9.1. Computation of a jet

The basic behaviour of jets has been studied by the author [9,10]. The result of a computer run is shown in Fig. 10. The motion of the cavity contour was obtained by a time-marching program. Before each time step a boundary value problem was solved to provide the velocities along the contour. Initially circular arc cavity is assumed, with zero normal velocity but non-zero circulation around the wedge and cavity. A narrow jet was obtained (Fig. 10). This is understandable. Once a fluid mass entered into the cavity of constant pressure, it continues its motion with constant velocity. This explains why a jet is formed, and that the jet velocity within the cavity is constant. It is interesting to note that the jet velocities obtained at various cavitation numbers were high, at about double of the steady jet velocities (Rjabouchinsky model). This indicates the strong tendency for the jet formations in cavities.

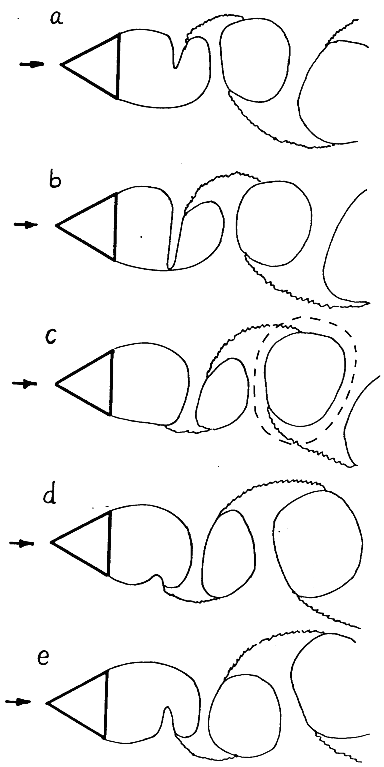

Fig. 9. Development of downward jet in the cavity [9]

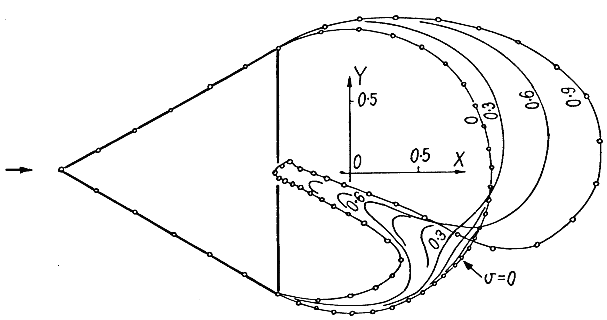

Fig. 10. Computed jet formation in a cavity [10], $K = 1$, $\Gamma = 6$, $x_{ref} = -10$, $\mathbf{v}_\infty = (1;0)$, $\Delta t = 0.05$.

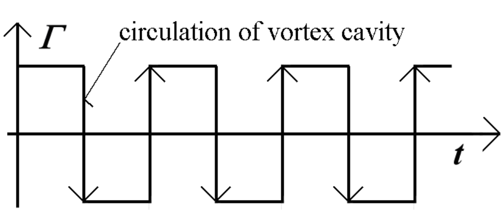

Fig. 11. The circulation around the wedge and main cavity versus time, in an inviscid flow scheme

For the complete cycle of the vortex formation (Fig. 9 is half) one may set up a frictionless scheme with the assumption that the circulation around the wedge and the main cavity change with time as shown in Fig. 11. When the jet touches the cavity surface (Fig. 9b) a vortex cavity is separated from the main cavity, taking circulation from the main cavity. Between vortex separations the flow is circulation preserving, $\boldsymbol{\Gamma}$ is constant. Thus $\boldsymbol{\Gamma}$ varies with time as in Fig. 11.

On wedge models the separation point is fixed. On circular cylinders it may oscillate. Nevertheless, according to the experiments the cavitating vortex formation mechanism is much the same for circular cylinders as for wedges (Fig. 9).

9.2. Non-cavitating Karman vortex rows

There is evidence that non-cavitating vortex rows are generated also by alternate jet formations:

a, Numerous pictures published on non-cavitating vortex rows show similar features as Fig. 9.

b, In the cavitation tunnel, operating at high cavitation number when the main cavity was not present but small cavities visualized the flow, the movement of the alternate jets was observed.

c, Theoretically, the pressure in the wake region is nearly constant as in the cavities. Thus the formation conditions of the jets are the same in both cases. The fluid mass in the non-cavitating wake naturally retards the movement of the jet, therefore jet velocities and the Strouhal numbers of the vortex separations are smaller.

9.3. Origin of vortex circulation

For non-cavitating flows several textbooks say that vortex circulation originates from the boundary layers. This is based on Kelvin's theorem. Vorticity cannot be generated within the practically inviscid fluid; therefore it must come from the boundary layer.

The theory of alternate jet formations offers another explanation. When the jet touches the cavity contour (Fig. 9b) the vortex cavity has a circulation. It is taken from the main cavity (Fig. 11), and neighboring jets continue to keep this circulation (dotted line in Fig. 9c).

Both explanations are valid, though the latter seems simpler and more general. In setting up an appropriate flow model, in which the vorticity can be calculated in the flow domain, Stokes theorem reads:

$$\int_C \mathbf{v}\,\mathbf{dr} = \int_S \mathrm{rot}\;\mathbf{v}\,\mathbf{dS} \quad . \qquad (4)$$

This indicates that any explanation based on the circulation (left side) can be converted to an explanation with vorticity (right side), and 'vice versa'.

10 Conclusion

For flow separations on curved boundaries the main elements of the flow mechanism are shown on Fig. 12. **A**, **B** and **C** are the points selected on Fig. 2a.

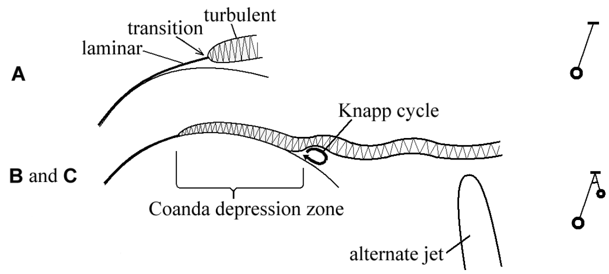

Fig. 12. Elements of flow separations

Laminar boundary layers (Case **A**) separate smoothly. The mechanism is determined mainly by the inertia of the flow. Alternate jet formations call upon the Karman vortex row.

With increasing Reynolds number, when the transition point approaches the surface, the turbulent boundary layer transports the mass out of the narrow region, and the resulted depression pulls the boundary layer to the surface, as in Coanda flow. The depression zones are seen on Fig. 2c. They are rather stable; this is a common experience with the lift of airplane wings.

Cavitation experiments show that at the downstream end of the depression zone a Knapp cycle is working. Vortex cavities are seen shed from this region. Damage tests (with lead) [8] also prove this. Maximum damage was found in two area: near the impacts of the alternate jets, and near the impacts of the small Knapp cycles.

The Knapp cycle explains also the irregular vortex shedding shown on Fig. 2b. The situation is similar to pendulums (shown on the right side of Fig. 12). In the case of laminar separation (**A**), the shedding frequency is definite. In cases of turbulent boundary layer separations (**B** and **C**) the main motion is still determined by the alternate jets, but the Knapp cycle (presumably with higher frequency) disturbs this, like in the case of two interconnected pendulums.

10.1 Factors affecting 2D flow separations

A summary is attempted. The physical factors dominant in 2D separations are:

a, The inertia of the fluid masses (Pelton jet, laminar separation).

b, The condition of the boundary layer near the separation zone (laminar or turbulent).

c, Depression zones (whether boundary allows them to come into being, and are they influenced or not).

10.2 The mechanism of vortex generation

Vortex formations which appear in essentially 2D flows are caused by jets:

a, for unidirectional vortex rows by the reentrant jets of the Knapp cycle,

b, for bidirectional vortex rows by the alternate jets.

Promising computation for flows around circular cylinders was shown by Meng Wang et al. [11]. The mechanical background of such flows shown above may help in future computations.

References

[1] Papers on 9th EUROMECH *European Turbulence Conference*, 2-5 July, 2002, Southampton, U.K.

[2] Batchelor, G.K., *An Introduction to Fluid Dynamics*, Cambridge University Press, 1970

[3] Roberson, J.A., Crowe, C.T., *Engineering Fluid Mechanics*, Houghton Mifflin Company, 1985

[4] Strscheletzky, M., Ein Beitrag zur Theorie des hydrodynamischen Gleichgewichtes von Strömungen, *VOITH Forschung*, Heft 2, August 1957, As 1

[5] Kaufmann, K., Grenzschichtbeeinflussung bei Diffusoren von Strömungsmaschinen, *VOITH Forschung*, Heft 2, August 1957, Aufsatz 2

[6] Knapp, R.T., Daily, J.W. and Hammitt, F.G. *Cavitation*, Mc Graw Hill, New York, 1970

[7] Furness, R.A., Studies of the mechanics of “fixed” cavities in two dimensional convergent-divergent nozzle, *Mechanical Engineers*, 1976, C160/74

[8] Varga, J., Sebestyén, Gy., Cavitation and cavitation erosion behind cylinder model, *ASME Cavitation Forum*, Detroit 1970, pp.38-40, also in *ASME Film Library*, also shown in *EUROMECH Colloquium 116*, Wageningen, 28-30 May 1979

[9] Fay, A.A., Explanation of how the Karman vortices are generated, *8th Conference on Fluid Machinery, Budapest*, 1987, pp. 211-218

[10] Fay, A.A., Computation of jet formations in wake cavities, *Symp. IAHR ‘Two phase flow and cavitation in power generation systems’*, Grenoble, 1976

[11] Meng Wang, Pietro Catalano, Giancula Iaccarino, Prediction of high Reynolds number flow over a circular cylinder using LES with wall modeling, *Center for Turbulence Research Briefs*, Stanford, 2001, pp 45 - 50